Research Square

Preprints are preliminary reports that have not undergone peer review.
They should not be considered conclusive, used to inform clinical practice,
or referenced by the media as validated information.

Coupling-scale invariance and mode-selective critical slowing in reduced Wong-Wang networks: exact fold geometry, spectral control, and stochastic observables

Majid Eshaghi Gorji

meshaghi@semnan.ac.ir

Semnan University

Nazanin Fereydouni Forouzande

Semnan University

Saeede Haghighatkhah

Semnan University

Research Article

Keywords: Wong–Wang model, saddle-node bifurcation, critical slowing down, global coupling, graph spectral gap

Posted Date: November 13th, 2026

DOI: https://doi.org/10.21203/rs.3.rs-11536843/v1

License: This work is licensed under a Creative Commons Attribution 4.0 International License.
Read Full License

Additional Declarations: No competing interests reported.

Coupling-scale invariance and mode-selective critical slowing in reduced Wong-Wang networks: exact fold geometry, spectral control, and stochastic observables

Majid Eshaghi Gorji[1*], Nazanin Fereydouni Forouzande[2] and Saeede Haghighatkhah[2]

[1*]Department of Mathematics and Computer Science, Semnan University, Semnan, Iran.
[2]Department of Cognitive Science, Semnan University, Semnan, Iran.

*Corresponding author(s). E-mail(s): meshaghi@semnan.ac.ir;
Contributing authors: nazaninfereydounif@gmail.com; haghighatkhahsaeede@gmail.com;

Abstract

Global coupling is widely used to organize collective dynamics in reduced neural mean-field models, but three quantities are often interpreted separately: the numerical value assigned to coupling, the bifurcation mechanism associated with that coupling, and the temporal statistics extracted from simulated activity. Here we establish an explicit mathematical link between these levels in the reduced Wong–Wang architecture. We first show that uniform rescaling of structural connectivity is exactly equivalent to reciprocal rescaling of global gain, so the magnitude of the coupling parameter is meaningful only after the connectivity normalization is specified. For connected symmetric regular networks, we then prove that a synchronized positive-coupling saddle-node is controlled by the Perron mode, while transverse modes remain stable and their damping is set by the graph spectral gap. Near a generic upper fold, the critical recovery time follows the universal law $\tau_{\mathrm{rec}} \sim K(G_c - G)^{-1/2}$; under isotropic weak noise, the same Jacobian spectrum determines modal variances and autocorrelation times. Numerical verification with the conventional reduced Wong–Wang parameterization and independent Euler–Maruyama simulations confirms these analytical predictions away from the immediate fold neighbourhood and identifies the finite-record regime in which nonlinear and sampling effects become important. The resulting framework is intentionally minimal: its contribution is not a new neural-mass model or a new empirical biomarker, but a reproducible mechanistic benchmark that separates coupling normalization, bifurcation geometry, topology-dependent recovery, and finite-time stochastic estimation within one commonly used neural mean-field architecture.

Keywords: Wong–Wang model; saddle-node bifurcation; critical slowing down; global coupling; graph spectral gap

1 Introduction

Reduced neural mean-field models occupy an important middle ground between microscopic network descriptions and large-scale brain models: they preserve a tractable nonlinear population dynamics while making collective regimes, stability changes and network effects analytically accessible (Wong and Wang 2006; Deco et al. 2013;

Spiegler et al. 2010; Cooray et al. 2023). In these models, a global coupling or gain parameter is often swept to organize transitions in simulated activity. Yet the numerical value of that parameter, the dynamical mechanism responsible for a transition, and the temporal statistics measured from the resulting trajectories are not interchangeable objects. A coupling value is defined relative to the connectivity matrix; a bifurcation is a property of the vector field and its Jacobian; and a finite-record timescale is an estimator whose value depends on the observation protocol. Precise connectivity conventions and model descriptions are therefore essential when quantitative comparisons are made across computational studies (Senk et al. 2022).

The reduced Wong–Wang family provides a particularly useful setting in which to make these distinctions explicit. Its nonlinear transfer function and slow synaptic variable have been used extensively in recurrent decision models and in large-scale descriptions of resting-state and ignition-like dynamics (Wong and Wang 2006; Deco et al. 2013; Castro et al. 2020). Bifurcation analysis supplies the natural language for identifying changes of stability in such systems (Kuznetsov 2004; Spiegler et al. 2010), while critical slowing down provides a mechanistic connection between approaching a transition and the increasing recovery time, variance and autocorrelation of fluctuations (Kuehn 2011; Meisel et al. 2015). At the same time, neural timescale estimates are known to depend on the estimator and observation window, so a temporal statistic should not be treated as a direct substitute for a dynamical eigenvalue (Murray et al. 2014; Zeraati et al. 2026). What is missing is a compact benchmark in which these layers are derived from the same equations and their boundaries are made explicit.

We address this gap with a deliberately minimal construction: two identical interacting mean-field units with reciprocal coupling, followed by an extension to connected symmetric regular graphs. The aim is not to introduce a new biological model or to claim that a two-node system represents a particular anatomical circuit. The aim is to expose, in a setting where every step can be proved and reproduced, how a coupling coordinate becomes a dynamical distance to a fold and how that fold controls temporal recovery. This design also makes a potentially confounding issue testable: the absolute value of a global gain cannot be interpreted independently of the normalization of structural connectivity.

The analysis is organized around four questions. First, which combination of structural connectivity and global gain is actually identifiable? Second, at a synchronized saddle-node, which network mode becomes critical and what controls the recovery of the remaining modes? Third, what scaling law follows from the local fold geometry, independently of any time-series statistic? Fourth, how faithfully do stochastic trajectory estimates recover the analytically predicted timescale when finite records and nonlinearities are introduced? We answer these questions in that order, moving from parameter identifiability to bifurcation geometry, from geometry to graph modes, and from graph modes to stochastic observables.

The main contribution is deliberately narrow. We prove an exact coupling-scale invariance, establish a mode-selective fold result for connected symmetric regular networks, derive the universal square-root divergence of the critical recovery time, and map the same Jacobian spectrum to the local Ornstein–Uhlenbeck statistics of weakly noisy trajectories. The numerical benchmark uses the established reduced Wong–Wang parameterization and independently regenerated Python outputs rather than fitted empirical data. This positioning distinguishes the present work from studies that use neural mass models primarily as phenomenological generators: here the model is used as an analytical benchmark for separating coupling normalization, bifurcation mechanism, topology-dependent slow modes and finite-time estimation. The resulting claims are correspondingly limited to the stated symmetry, regularity and local-noise assumptions.

This separation is important for interpretation. A long empirical or simulated correlation time is not, by itself, evidence that a system is approaching a bifurcation; a small graph spectral gap can generate a slow but still stable transverse mode, while a finite record can bias an estimator near a genuine critical mode. Conversely, a fold identified from the equilibrium equations has a precise local mechanism even before any stochastic statistic is computed. By placing these statements in one analytical chain, the study provides a compact reference point against which

more heterogeneous, directed, delayed or empirically constrained neural-network models can later be compared.

2 Model and analytical framework

The reduced Wong-Wang family originates from a reduction of recurrent spiking-network dynamics to a slow synaptic gating variable (Wong and Wang 2006) and has subsequently been used in large-scale models of resting and ignition-like brain dynamics (Deco et al. 2013; Castro et al. 2020). We consider two identical populations with gating variables $S_1, S_2 \in (0,1)$ and reciprocal coupling weight $c > 0$:

$$dS_1 = F_1(S_1, S_2; G)\,dt + \sigma\,dW_1, \tag{1}$$
$$dS_2 = F_2(S_1, S_2; G)\,dt + \sigma\,dW_2, \tag{2}$$

where W_1, W_2 are independent standard Wiener processes and

$$F_1 = -\frac{S_1}{\tau_s} + (1 - S_1)\gamma H(x_1), \tag{3}$$
$$x_1 = J_N\big(wS_1 + GcS_2\big) + I_0,$$
$$F_2 = -\frac{S_2}{\tau_s} + (1 - S_2)\gamma H(x_2), \tag{4}$$
$$x_2 = J_N\big(wS_2 + GcS_1\big) + I_0.$$

with

$$H(x) = \frac{ax - b}{1 - \exp[-d(ax - b)]}. \tag{5}$$

This parameterization follows established reduced Wong–Wang implementations, while the reciprocal-edge normalization is an explicit modelling convention rather than an empirical connectivity estimate (Wong and Wang 2006; Deco et al. 2013; Castro et al. 2020). The removable singularity at $ax = b$ is evaluated using the limit $H(b/a) = 1/d$; the supplementary code uses an `expm1`-based implementation to avoid cancellation. The standard parameter values used for the deterministic benchmark are listed in Table 1. Importantly, $c = 1$ is a normalization convention for the two-node example rather than an empirical anatomical measurement, while σ controls only the small-noise verification and is not fitted to data.

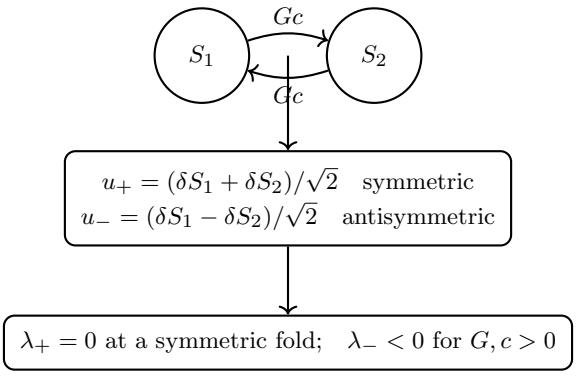


Fig. 1 The two-node model and the symmetry-adapted perturbation coordinates. At a positive-coupling symmetric saddle-node the symmetric mode is critical while the antisymmetric mode remains linearly stable

Fig. 1 separates the network coordinates from their symmetry-adapted modes. That change of basis is not cosmetic: it is the key step that makes the critical direction and the stochastic observables transparent.

Because the equations are invariant under exchange $S_1 \leftrightarrow S_2$, the diagonal subspace $\mathcal{D} = \{S_1 = S_2\}$ is invariant. Writing $S_1 = S_2 = S$ gives the scalar deterministic equation

$$\begin{aligned}\dot{S} &= F(S; G) \\ &= -\frac{S}{\tau_s} + (1 - S)\gamma H(J_N(w + cG)S + I_0)\,.\end{aligned} \tag{6}$$

A symmetric equilibrium S^* satisfies $F(S^*; G) = 0$. A nondegenerate fold additionally satisfies

$$\begin{aligned} F_S(S_c; G_c) &= 0, \\ F_{SS}(S_c; G_c) &\neq 0, \\ F_G(S_c; G_c) &\neq 0. \end{aligned} \tag{7}$$

The full Jacobian at a symmetric equilibrium has the form

$$J = \begin{pmatrix} A & B \\ B & A \end{pmatrix}, \quad B = (1 - S^*)\gamma H'(x^*) J_N G c, \tag{8}$$

where

$$A = -\tau_s^{-1} - \gamma H(x^*) + (1 - S^*)\gamma H'(x^*) J_N w. \tag{9}$$

Table 1 Model parameters. The transfer and kinetic values follow established reduced Wong-Wang implementations; the reciprocal edge normalization and the small-noise level are declared modelling choices, not empirical estimates.

Symbol	Value	Unit	Status/source
a	270	Hz nA^{-1}	Reduced Wong-Wang parameterization (Deco et al. 2013; Castro et al. 2020)
b	108	Hz	Reduced Wong–Wang parameterization (Deco et al. 2013; Castro et al. 2020)
d	0.154	s	Reduced Wong–Wang parameterization (Deco et al. 2013; Castro et al. 2020)
γ	0.641	–	NMDA gating factor (Deco et al. 2013; Castro et al. 2020)
τ_s	0.1	s	Synaptic time constant (Deco et al. 2013; Castro et al. 2020)
J_N	0.2609	nA	Synaptic coupling scale (Deco et al. 2013; Castro et al. 2020)
w	0.9	–	Local recurrence used in the ignition implementation (Castro et al. 2020)
I_0	0.3	nA	Baseline input used in the ignition implementation (Castro et al. 2020)
c	1	–	Unit normalization of the reciprocal two-node edge
σ	0.001	s$^{-1/2}$	Small-noise numerical verification; not data-fitted

Hence, the symmetry-adapted eigenvalues are

$$\begin{aligned} \lambda_+ &= A + B = F_S(S^*; G), \\ \lambda_- &= A - B = \lambda_+ - 2B. \end{aligned} \tag{10}$$

For the transfer function in Eq. (5), $H'(x) > 0$ over the relevant domain, the accompanying code evaluates the derivative directly and verifies this at all reported equilibria.

Theorem 1 (Mode selectivity of a positive-coupling symmetric fold) *Suppose $G_c > 0$, $c > 0$, $0 < S_c < 1$, $J_N > 0$, $\gamma > 0$, and $H'(x_c) > 0$. If (S_c, G_c) is a symmetric fold satisfying $\lambda_+(S_c, G_c) = 0$, then*

$$\lambda_-(S_c, G_c) = -2(1 - S_c)\gamma H'(x_c) J_N G_c c < 0. \tag{11}$$

The centre eigenspace is one-dimensional and symmetric; the antisymmetric mode is strictly stable.

Proof At a symmetric equilibrium the Jacobian is Eq. (8), so its eigenvectors are $(1, 1)^\top/\sqrt{2}$ and $(1, -1)^\top/\sqrt{2}$ with eigenvalues $\lambda_+ = A + B$ and $\lambda_- = A - B$. At a symmetric fold, $\lambda_+ = 0$, hence $A = -B$. Substitution gives $\lambda_- = A - B = -2B$. Every factor in $B = (1 - S_c)\gamma H'(x_c) J_N G_c c$ is strictly positive under the hypotheses, so $B > 0$ and therefore $\lambda_- < 0$. No additional numerical stability assumption is required. □

The theorem strengthens the usual statement that a fold exists: it identifies which collective perturbation becomes slow. It also implies a useful stability ordering. Whenever a symmetric equilibrium has $\lambda_+ < 0$ a positive coupling, Eq. (10) gives $\lambda_- < \lambda_+ < 0$, so the full two-dimensional equilibrium is linearly stable. Thus, no hidden antisymmetric instability can precede the symmetric fold in this two-node architecture.

A second issue concerns the interpretation of G. Whole-brain models normally define a structural matrix first and then multiply it by a global gain. The numerical value of that gain is therefore inseparable from the normalization of the structural weights. In the present two-node reduction this statement can be made exact.

Proposition 1 (Exact connectivity-scale/global-gain invariance) *Consider the N-node reduced Wong-Wang system*

$$x_i = J_N \left(w S_i + G \sum_{j=1}^{N} C_{ij} S_j \right) + I_0. \tag{12}$$

For every $\alpha > 0$, the transformation

$$C \mapsto \alpha C, \qquad G \mapsto G/\alpha \tag{13}$$

leaves the complete deterministic vector field and, for unchanged noise law, the complete stochastic differential equation invariant. Hence the absolute scale G is structurally non-identifiable unless a normalization convention for C is fixed.

Proof Under Eq. (13),

$$\frac{G}{\alpha}\sum_j(\alpha C_{ij})S_j = G\sum_j C_{ij}S_j$$

for every state S and every node i. Therefore, every input x_i, every drift component, and every Jacobian entry is unchanged. Because the diffusion term is also unchanged, the stochastic law is identical. Thus any deterministic trajectory, equilibrium, bifurcation point, transition probability, or time-series statistic generated by the model is invariant under the paired rescaling. Only the product GC is identified by the model equations. □

For the reciprocal pair $C_{12} = C_{21} = c$, this proposition reduces to the relation $w + cG$ on the symmetric branch and gives

$$G_c(c) = \frac{\kappa_c - w}{c}, \tag{14}$$

where κ_c is the effective recurrent coefficient at the fold. The point is not that G is useless, but that its numerical magnitude is meaningful only relative to a stated connectivity normalization. This is especially important when comparing studies that rescale, threshold or otherwise transform structural matrices (Senk et al. 2022).

This proposition does not imply that global coupling is meaningless; it states the narrower and practically important point that its numerical value is conditional on a declared connectivity normalization. Comparisons of G across models are therefore scientifically interpretable only when the scaling of the corresponding structural matrices is fixed or transformed explicitly.

The local slowing-down law follows from the same fold geometry. Let $\mu = G_c - G > 0$ denote the distance to the upper fold along the stable low-activity branch. Taylor expansion of F about (S_c, G_c) yields

$$0 = -F_G\mu + \frac{1}{2}F_{SS}(S - S_c)^2 + \mathcal{O}(\mu^{3/2}), \tag{15}$$

where derivatives are evaluated at the fold. For the upper fold in Table 2, $F_G > 0$ and $F_{SS} > 0$, and the low stable branch takes the negative square-root displacement. Therefore

$$\lambda_+ = F_S = -\sqrt{2F_GF_{SS}}\,\mu^{1/2} + \mathcal{O}(\mu), \tag{16}$$

so the deterministic local recovery time is

$$\begin{aligned}\tau_{\text{rec}} = -\lambda_+^{-1} &= K\mu^{-1/2} + \mathcal{O}(1),\\ K &= \frac{1}{\sqrt{2F_GF_{SS}}}.\end{aligned} \tag{17}$$

The square-root law is the standard local saddle-node scaling from bifurcation theory (Kuznetsov 2004; Kuehn 2011); here the derivation identifies its model-specific prefactor and makes clear that the scaling is a property of the vector field rather than a regression assumption. The same scaling logic has been used experimentally to distinguish transition mechanisms in neuronal spiking (Meisel et al. 2015).

The stochastic consequence is equally direct. Linearize Eq. (2) around a stable symmetric equilibrium and rotate the independent Brownian motions into $W_\pm = (W_1 \pm W_2)/\sqrt{2}$. Orthogonality preserves independence, giving

$$\begin{aligned}du_+ &= \lambda_+u_+\,dt + \sigma\,dW_+,\\ du_- &= \lambda_-u_-\,dt + \sigma\,dW_-.\end{aligned} \tag{18}$$

Each mode is therefore an Ornstein–Uhlenbeck process. For $\lambda_\pm < 0$,

$$\begin{aligned}\text{Var}(u_\pm) &= \frac{\sigma^2}{-2\lambda_\pm},\\ \text{Corr}[u_\pm(t), u_\pm(t+h)] &= e^{\lambda_\pm h}.\end{aligned} \tag{19}$$

Because λ_- remains bounded away from zero at the fold whereas $\lambda_+ \to 0^-$, the symmetric-mode variance and correlation time diverge in the linear approximation while the antisymmetric quantities remain finite. Writing $V_\pm = \text{Var}(u_\pm)$ and reverting to (S_1, S_2) gives

$$\text{Corr}(S_1, S_2) = \frac{V_+ - V_-}{V_+ + V_-} \longrightarrow 1 \quad \text{as} \quad G \to G_c^-. \tag{20}$$

Thus, the same eigenvalue that governs deterministic recovery also predicts an increasingly shared fluctuation mode. The result is local and small-noise: it does not assert that the full nonlinear stochastic system has a stationary Gaussian distribution arbitrarily close to the fold, where basin escape and finite-record effects become important.

The same analytical structure extends beyond the reciprocal pair to connected symmetric regular networks. This extension is useful because

standard graph-theoretic results make clear which part of the dynamics is controlled by the row sum and which part is controlled by the remaining spectrum (Chung 1997; Senk et al. 2022).

The two-population calculation is transparent, but the mechanism is not restricted to two nodes. Consider N identical reduced Wong–Wang units with a real symmetric, nonnegative connectivity matrix C satisfying $C_{ii} = 0$. Assume the graph is connected and regular, so

$$C\mathbf{1} = r\mathbf{1}, \qquad r > 0, \tag{21}$$

where r is the common row sum. The synchronized subspace $S_1 = \cdots = S_N = S$ is then invariant and obeys

$$\dot{S} = -\frac{S}{\tau_s} + (1-S)\gamma H(J_N(w + Gr)S + I_0)\,. \tag{22}$$

Thus the location of a synchronized fold depends on the network through the row sum r, whereas transverse stability depends on the remaining graph eigenvalues.

Let $r = \nu_1 > \nu_2 \geq \cdots \geq \nu_N$ denote the eigenvalues of C. Connectedness and nonnegativity imply that $\nu_1 = r$ is simple by Perron-Frobenius theory (Chung 1997). At a synchronized equilibrium the Jacobian can be written

$$J^{\mathrm{lin}} = a_0 I + \beta C, \qquad \beta = (1-S)\gamma H'(x) J_N G > 0, \tag{23}$$

as follows:

$$a_0 = -\tau_s^{-1} - \gamma H(x) + (1-S)\gamma H'(x) J_N w. \tag{24}$$

Hence the graph eigenvectors diagonalize the neural linearization and

$$\lambda_k = a_0 + \beta\nu_k, \qquad k = 1, \ldots, N. \tag{25}$$

Theorem 2 (Unique critical Perron mode at a synchronized fold) *Under the assumptions above, suppose a synchronized equilibrium undergoes a positive-coupling saddle-node so that $\lambda_1 = 0$. Then*

$$\lambda_k = \beta(\nu_k - r) < 0, \qquad k = 2, \ldots, N. \tag{26}$$

Therefore the centre eigenspace is one-dimensional and spanned by the synchronized Perron vector $\mathbf{1}$. No transverse graph mode is critical at the fold.

Proof At the fold, $\lambda_1 = a_0 + \beta r = 0$, so $a_0 = -\beta r$. Substitution into Eq. (25) gives $\lambda_k = \beta(\nu_k - r)$. Because $\beta > 0$ and the connected nonnegative regular matrix has the simple Perron eigenvalue $\nu_1 = r$ with $\nu_k < r$ for every $k \geq 2$, all transverse eigenvalues are strictly negative. □

The theorem yields a quantitative topological refinement. Define the adjacency spectral gap

$$\delta = r - \nu_2 > 0. \tag{27}$$

Then the slowest transverse eigenvalue at the fold is

$$\lambda_{\mathrm{tr}} = -\beta_c \delta. \tag{28}$$

Consequently, the synchronized fold can be identical for two row-sum-matched networks while the separation between the critical timescale and the slowest noncritical timescale differs strongly. This point matters for neural-timescale interpretation: a small graph spectral gap can generate long but noncritical transverse relaxation, whereas the actual fold is still carried only by the Perron mode.

Corollary 1 (Modal Ornstein–Uhlenbeck decomposition) *If the additive noise is isotropic, $dS = F(S)\,dt + \sigma\,dW$, the orthogonal eigenbasis of a symmetric C transforms the linearized stochastic system into independent scalar Ornstein–Uhlenbeck modes*

$$du_k = \lambda_k u_k\,dt + \sigma\,dB_k. \tag{29}$$

For a fixed connected regular graph, as $G \to G_c^-$ the stationary covariance is asymptotically dominated by the Perron mode. Because that mode is proportional to $\mathbf{1}$, pairwise correlations approach one within the local linear approximation.

This result provides a clean hierarchy of statements. The fold location on the synchronized branch is controlled by rG; the global scale of G is redundant with the global scale of C; and the transverse recovery hierarchy is controlled by the non-Perron spectrum. These are distinct pieces of information and should not be collapsed into a single fitted coupling number.

3 Numerical and stochastic verification

The numerical checks below are designed to test the analytical claims rather than replace

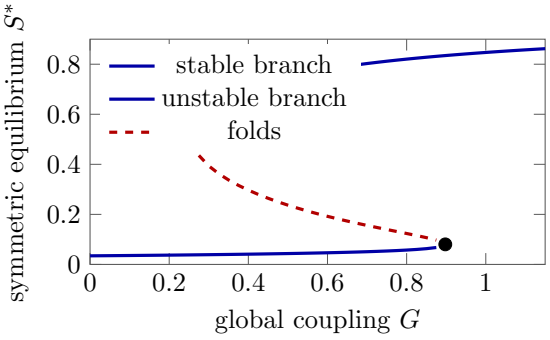


Fig. 2 Symmetric equilibrium branch of the two-population model. The coarse plotted coordinates are only for visualization; the fold coordinates in Table 2 are obtained by solving the simultaneous nonlinear equations $F = F_S = 0$. The full stability of every solid symmetric branch follows from $\lambda_- < \lambda_+$ for $G > 0$

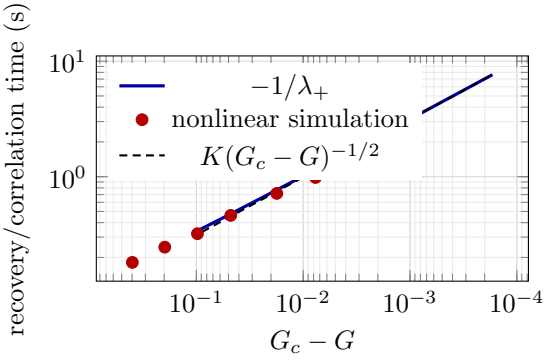


Fig. 3 Critical slowing down at the upper fold. The deterministic local recovery time approaches the saddle-node asymptote. Finite nonlinear simulations agree well over the resolved regime and underestimate the increasingly long time constant closest to the fold, where the fixed record contains fewer effective correlation lengths

them with curve fitting; critical slowing and estimator-dependent deviations are interpreted in the context of established bifurcation and neural-timescale literature (Kuznetsov 2004; Kuehn 2011; Meisel et al. 2015; Murray et al. 2014). The analytical results do not require numerical continuation, but a numerical benchmark is useful both to locate the folds for the literature parameterization and to test the finite-sample behavior of the stochastic observables.All numbers in this section are regenerated by the accompanying Python code (see Code availability); no external empirical dataset is required. Solving $F = F_S = 0$ with the parameters in Table 1 and $c = 1$ yields two symmetric folds (Table 2). The lower fold creates a stable high-activity branch together with an unstable middle branch. The upper fold annihilates the stable low branch and the unstable middle branch. Between the two points the deterministic system is bistable. At both folds the antisymmetric eigenvalue is strictly negative, in agreement with the theorem.

At the upper fold, the numerical derivatives are $F_G = 0.4849137503$ and $F_{SS} = 105.0656724$, which yield the prefactor $K = 0.09906548\,\mathrm{s}$ in Equation (17). A log–log regression of the deterministic local recovery time over the selected branch points $G \in [0.80, 0.8975]$ yields an estimated slope of -0.4896. As the fitting interval is restricted toward the fold, the estimated slope approaches $-1/2$, consistent with the contribution of higher-order terms away from the asymptotic regime. The fold is located independently by solving Equation (7), and the scaling law is evaluated afterward as a consistency check.

For the direct stochastic check, we use Euler–Maruyama with $\Delta t = 1$ ms, 30 s per realization, a 5 s burn-in, 32 independent realizations per G, $\sigma = 0.001$, and fixed master seed 20260927. Observables are computed from the symmetric coordinate sampled every 10 ms after burn-in. The empirical correlation time is obtained from the lag-10 ms correlation by $\widehat{\tau} = -\Delta/\log\widehat{\rho}(\Delta)$, avoiding a multi-parameter nonlinear ACF fit. Table 3 shows that the nonlinear simulations track the linear OU prediction well away from the immediate fold neighborhood. The discrepancy grows closest to G_c, precisely where a finite trajectory covers too few recovery times and the nonlinear fold geometry becomes harder to approximate by a stationary local Gaussian process. We treat that discrepancy as a validity boundary, not as a quantity to tune away.

The structural-scale result can also be visualized without further simulation. Because the effective coefficient $\kappa = w + cG$ is the quantity that enters the symmetric equation, both fold gains vary exactly as $1/c$ (Fig. 4). This provides a direct reason not to report a global coupling value as though it were a model-independent physical constant.

The network theorem yields a second consequence for network dynamics without requiring anatomical data. When each regular graph is normalized so that its connectivity matrix has row

Table 2 Numerically computed fold points on the symmetric branch under the unit edge-weight convention $c = 1$. The residuals of $F = 0$ and $F_S = 0$ are below 10^{-11}, as verified by the accompanying code.

Fold	G_c	S_c	λ_- (s^{-1})	Interpretation
Lower	0.2547375424	0.5198814960	−9.189486	high/middle branches appear
Upper	0.8976692317	0.0801818818	−10.857619	low/middle branches disappear

Table 3 Small-noise verification on the stable low-activity branch. Simulation estimates are averaged across 32 realizations generated using a fixed master seed. Standard deviations and additional variance diagnostics are reported in Online Resource 1.

G	τ_{th} (s)	$\widehat{\tau}$ (s)	$\rho_{12,\mathrm{th}}$	$\widehat{\rho}_{12}$	λ_- (s^{-1})
0.500	0.1807	0.1812	0.2409	0.2517	-9.0489
0.700	0.2463	0.2455	0.4109	0.4124	-9.7261
0.800	0.3403	0.3209	0.5512	0.5224	-10.1578
0.850	0.4768	0.4623	0.6651	0.6363	-10.4274
0.880	0.7681	0.7169	0.7819	0.7647	-10.6342
0.890	1.1539	0.9843	0.8505	0.8202	-10.7257
0.895	1.9400	1.3921	0.9088	0.8626	-10.7875

Table 4 Effect of network topology on the slowest transverse recovery time at the upper synchronized fold. All networks are normalized to have a connectivity-matrix row sum of one and consequently share the same synchronized fold, $G_c = 0.8976692$.

Network	ν_2	$\delta = 1 - \nu_2$	λ_{tr} (s^{-1})	τ_{tr} (s)
Two-node edge	−1.0000	2.0000	−10.8576	0.0921
$K_8/(7)$	−0.1429	1.1429	−6.2044	0.1612
$C_8/2$	0.7071	0.2929	−1.5901	0.6289
$C_{16}/2$	0.9239	0.0761	−0.4132	2.4199
$C_{32}/2$	0.9808	0.0192	−0.1043	9.5865

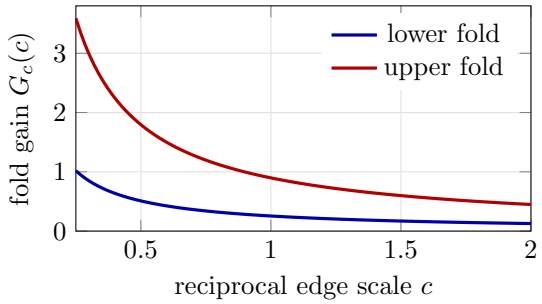


Fig. 4 Exact dependence of the two fold gains on the arbitrary scale of the reciprocal structural edge. The state-space fold is fixed by the effective coefficient $w + cG$; rescaling c rescales the reported G_c inversely

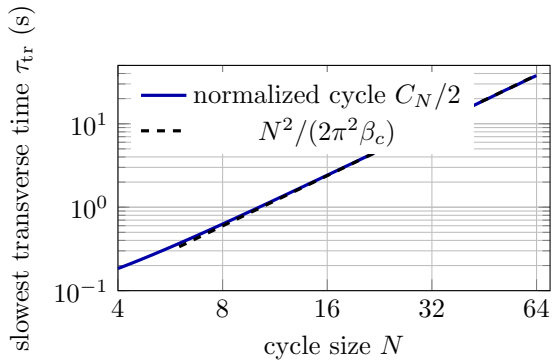


Fig. 5 A synchronized fold need not imply a single practically relevant timescale. For normalized cycles the graph spectral gap closes as $1 - \cos(2\pi/N) \sim 2\pi^2/N^2$, so the slowest transverse recovery grows as N^2 even though that mode never becomes critical for any fixed connected cycle

sum $r = 1$, Equation (22) is identical across the considered graphs. Consequently, the two synchronized fold locations remain unchanged from those reported in Table 2, whereas the transverse spectrum varies with network topology. At the upper fold, $\beta_c = 5.4288094\,s^{-1}$. For a network consisting of two nodes connected by a single edge, $\delta = 2$, giving a transverse eigenvalue of $-10.8576\,s^{-1}$. For a normalized complete graph K_N, $\delta = N/(N-1)$, whereas for a normalized cycle C_N, $\delta = 1 - \cos(2\pi/N)$. For the cycle, δ scales as $\mathcal{O}(N^{-2})$, so the slowest transverse mode becomes progressively less strongly damped as network size increases, even though the synchronized bifurcation remains unchanged.

These synthetic graph calculations are not intended to substitute for connectome-based analysis. Instead, they provide a controlled illustration of a limitation in interpreting long correlation times: such timescales need not arise solely from the critical eigenmode. Depending on network topology, the connectivity spectrum can also support slowly relaxing but stable transverse modes.

Under the assumptions of the modal decomposition derived above, these contributions can be distinguished analytically before fitting the model to empirical data.

4 Discussion

The central result is the separation of four factors that can otherwise be treated as a single phenomenon: connectivity normalization, local bifurcation geometry, the network-mode spectrum, and the estimator applied to finite stochastic trajectories. Reduced Wong–Wang models provide an established and tractable neural mean-field framework (Wong and Wang 2006; Deco et al. 2013; Castro et al. 2020). The contribution of the present study is to use this framework as a controlled analytical benchmark. In the two-node system, the fold is located by solving the equilibrium and degeneracy conditions, rather than inferred from a signal statistic. This analysis also identifies the critical eigenmode, while the local normal form yields the square-root scaling of the recovery time. The resulting mechanistic chain places the fold geometry upstream of the predicted temporal slowing: the slowing follows from the bifurcation structure rather than defining the fold itself.

The first implication concerns the meaning of global coupling. Because the input depends on the product GC, a uniform transformation $C \mapsto \alpha C$ and $G \mapsto G/\alpha$ leaves the model unchanged. The absolute numerical value of G is therefore not invariant under a change of connectivity normalization. This is a mathematical identifiability statement, not an empirical claim about anatomical connectivity. It matters whenever coupling values are compared across simulations or across whole-brain implementations, because a number quoted without its matrix normalization does not define a unique dynamical operating point. Precise connectivity conventions have likewise been identified as an important component of reproducible neuronal network modelling (Senk et al. 2022).

The second implication concerns which mode actually slows. For connected symmetric regular coupling, the synchronized equilibrium reduces the network Jacobian to graph eigenmodes. At a positive-coupling synchronized fold, the Perron mode reaches zero first, whereas transverse modes retain negative eigenvalues. Thus the divergent recovery time is associated with one collective direction, while the graph spectral gap determines how close the slowest transverse mode can come to it. The normalized-cycle example makes the distinction transparent: the synchronized fold remains unchanged with network size, but the slowest stable transverse relaxation increases as the spectral gap closes. A long timescale can therefore have two mathematically distinct origins—critical slowing of the Perron mode or topology-induced slowing of a stable transverse mode. This distinction is relevant to interpretation of neural timescales, for which multiple estimators and dynamical sources can produce non-equivalent numerical values (Murray et al. 2014; Zeraati et al. 2026).

A further methodological implication follows from the analysis. Near a generic upper saddle-node, the recovery time scales asymptotically as $\tau_{\mathrm{rec}} \sim K(G_c - G)^{-1/2}$, where the prefactor is determined by local derivatives of the vector field. The exponent follows from the saddle-node normal form rather than from an empirical fit used to locate the transition (Kuznetsov 2004; Kuehn 2011). The complementary stochastic analysis shows that, under a local linearization and weak additive noise, the dynamics decompose into Ornstein–Uhlenbeck modes. Within this approximation, the modal eigenvalues and noise covariance jointly determine the variance and autocorrelation structure. The simulations therefore serve to check the analytical predictions and assess the limitations imposed by finite observation records; they are not presented as evidence for a new statistical biomarker. This interpretation is consistent with previous work relating critical slowing down to changes in recovery, variance and autocorrelation near dynamical transitions (Meisel et al. 2015).

These results further clarify the role of the temporal index used in this study. The index should be interpreted as a compact secondary descriptor of trajectory-level temporal organization, rather than as an independent criterion for criticality or a validated biological biomarker. Its purpose is to assess whether a trajectory-derived quantity behaves consistently with a dynamical mechanism identified independently from the Jacobian. Near the fold, deviations from the local prediction are expected as nonlinear drift, excursions beyond the local region of validity, and finite

observation windows weaken the assumptions underlying the stationary local Gaussian approximation. Such deviations should be interpreted as limitations of the approximation and estimation procedure, rather than eliminated through parameter tuning. Finite-record estimates and local eigenvalues characterize related but distinct aspects of the dynamics.

The conclusions are restricted to the assumptions and scope of the present model. The formulation uses identical units, instantaneous reciprocal coupling, and independent additive noise; it does not incorporate anatomical heterogeneity, transmission delays, inhibition, hemodynamics, or an explicit measurement model. The network theorem additionally assumes connected, symmetric, nonnegative coupling, identical local dynamics, and constant row sums. Outside these conditions, synchronization and an orthogonal graph-mode decomposition are not guaranteed, so the critical direction must be determined from the Jacobian of the system under consideration. The stochastic analysis is local and does not provide a quantitative account of noise-induced switching, basin escape, or residence-time distributions. Because the study uses no human, animal, or connectome dataset, its findings do not establish empirical, diagnostic, or clinical validity. The results should therefore be interpreted as a theoretical benchmark within the stated assumptions.

The natural next tests follow directly from those boundaries. Full two-parameter continuation can determine how the fold set deforms when the connectivity weight, recurrent gain or other model parameters are varied jointly. Heterogeneous and directed networks can test how the Perron-mode result changes when exact symmetry is broken, while delayed coupling can determine whether another instability such as a Hopf bifurcation pre-empts the fold. A separate stochastic basin analysis could quantify first-passage and switching rates beyond the local Ornstein–Uhlenbeck regime. These extensions should be treated as new questions rather than retroactively incorporated into the present claims. Their value is precisely that the current benchmark provides an analytically specified reference case against which such departures can be measured.

Overall, the study establishes a compact mechanistic chain rather than introducing a new neural-mass architecture. Connectivity normalization determines how the global gain should be interpreted; the effective coupling sets the system's position relative to the fold; at the synchronized fold, the Perron-mode eigenvalue reaches zero; and the graph spectrum determines the damping of the remaining transverse modes. Under weak noise, these modal properties constrain the temporal statistics of the simulated trajectories. By deriving the analytical results from a common mathematical formulation and providing code to reproduce the reported computations, the study aims to establish a reproducible theoretical benchmark for investigating coupling-dependent temporal organization while distinguishing bifurcation mechanisms, network topology, and finite-record estimation effects.

5 Conclusion

We have shown that coupling-dependent temporal organization in a reduced Wong–Wang network can be understood through a single, explicit dynamical chain. The absolute global gain is meaningful only relative to a declared connectivity normalization. For connected symmetric regular networks, the synchronized positive-coupling fold is controlled by the Perron mode, while the graph spectral gap determines the damping of the remaining stable modes. Near a generic upper fold, the critical recovery time follows the universal square-root law, and weak stochastic fluctuations inherit the same modal structure through their variances and autocorrelation times.

The significance of the framework is therefore not the introduction of another neural-mass model or another standalone temporal index. It is the separation of mechanisms that can otherwise produce superficially similar long timescales: genuine critical slowing, topology-induced slow stable modes, and finite-record estimation effects. The resulting benchmark is intentionally minimal and analytically transparent, providing a reproducible baseline for future studies that add heterogeneity, directed or delayed coupling, empirical connectivity, or stochastic switching dynamics.

Declarations

Funding. The authors did not receive support from any organization for the submitted work.

Competing interests. The authors have no relevant financial or non-financial interests to disclose.

Ethics approval. Not applicable. No human participants, animal subjects, or identifiable personal data were involved in this study.

Consent to participate and to publish. Not applicable.

Data availability. No external human, animal, or connectome dataset was used in this study. Model parameters obtained from the literature are cited in Table 1, while modelling assumptions, normalization conventions, and simulation-design choices are identified separately. All numerical results, equilibrium branch points, figures, tables, and stochastic verification outputs (CSV files and figure files) are generated from the model equations in Eqs. (2)–(5) by the code described below, and are archived together with it at https://doi.org/10.5281/zenodo.23495771.

Code availability. The standalone Python reproduction package, including the executable source code, dependency specifications, random-seed configuration, and an audit record linking reported numerical results to their computational outputs, is available at https://github.com/thenewcomershk-lab/wong-wang-coupling (current version), and the version used for this manuscript is archived at https://doi.org/10.5281/zenodo.23495771.

Author contributions. Conceptualization: M.E.G.; Formal analysis: M.E.G.; Software: M.E.G.; Supervision: M.E.G.; Writing – original draft: S.H., N.F.F.; Writing – review & editing: S.H., N.F.F. All authors read and approved the final manuscript.

Supplementary information. Online Resource 1 (PDF) provides mathematical derivations, the computational protocol, standard deviations, and additional variance diagnostics.

References

Castro, S., El-Deredy, W., Battaglia, D., and Orio, P. (2020). Cortical ignition dynamics is tightly linked to the core organisation of the human connectome. *PLoS Computational Biology*, 16(7), e1007686. doi:10.1371/journal.pcbi.1007686.

Chung, F. R. K. (1997). *Spectral Graph Theory*. CBMS Regional Conference Series in Mathematics, Vol. 92. American Mathematical Society.

Cooray, G. K., Rosch, R. E., and Friston, K. J. (2023). Global dynamics of neural mass models. *PLoS Computational Biology*, 19(2), e1010915. doi:10.1371/journal.pcbi.1010915.

Deco, G., Ponce-Alvarez, A., Mantini, D., Romani, G. L., Hagmann, P., and Corbetta, M. (2013). Resting-state functional connectivity emerges from structurally and dynamically shaped slow linear fluctuations. *Journal of Neuroscience*, 33(27), 11239–11252. doi:10.1523/JNEUROSCI.1091-13.2013.

Kuehn, C. (2011). A mathematical framework for critical transitions: bifurcations, fast–slow systems and stochastic dynamics. *Physica D: Nonlinear Phenomena*, 240(12), 1020–1035. doi:10.1016/j.physd.2011.02.012.

Kuznetsov, Y. A. (2004). *Elements of Applied Bifurcation Theory*, 3rd ed. Springer. doi:10.1007/978-1-4757-3978-7.

Meisel, C., Klaus, A., Kuehn, C., and Plenz, D. (2015). Critical slowing down governs the transition to neuron spiking. *PLoS Computational Biology*, 11(2), e1004097. doi:10.1371/journal.pcbi.1004097.

Murray, J. D., Bernacchia, A., Freedman, D. J., Romo, R., Wallis, J. D., Cai, X., Padoa-Schioppa, C., Pasternak, T., Seo, H., Lee, D., and Wang, X.-J. (2014). A hierarchy of intrinsic timescales across primate cortex. *Nature Neuroscience*, 17, 1661–1663. doi:10.1038/nn.3862.

Senk, J., Kriener, B., Djurfeldt, M., Voges, N., Jiang, H.-J., Schüttler, L., Gramelsberger, G., Diesmann, M., Plesser, H. E., and van Albada, S. J. (2022). Connectivity concepts in neuronal network modeling. *PLoS Computational Biology*, 18(9), e1010086. doi:10.1371/journal.pcbi.1010086.

Spiegler, A., Kiebel, S. J., Atay, F. M., and Knösche, T. R. (2010). Bifurcation analysis of neural mass models: impact of

extrinsic inputs and dendritic time constants. *NeuroImage*, 52(3), 1041–1058. doi:10.1016/j.neuroimage.2009.12.081.

Wong, K.-F. and Wang, X.-J. (2006). A recurrent network mechanism of time integration in perceptual decisions. *Journal of Neuroscience*, 26(4), 1314–1328. doi:10.1523/JNEUROSCI.3733-05.2006.

Zeraati, R., Levina, A., Macke, J. H., and Gao, R. (2026). Neural timescales from a computational perspective. *Nature Neuroscience*, 29, 1534–1547. doi:10.1038/s41593-026-02343-8.

Supplementary Files

This is a list of supplementary files associated with this preprint. Click to download.

- supplementary1.pdf